https://doi.org/10.1016/j.jcsr.2018.06.007

Material properties and residual stresses of octagonal high strength steel hollow sections

Han Fang[a], Tak-Ming Chan[a,*] and Ben Young[b]

[a]Department of Civil and Environmental Engineering, The Hong Kong Polytechnic University, Hung Hom, Hong Kong, China

[b]Department of Civil Engineering, The University of Hong Kong, Pokfulam Road, Hong Kong, China

*tak-ming.chan@polyu.edu.hk

Abstract

This paper presents an experimental investigation to quantify the variation of material properties and residual stresses in the octagonal high strength steel hollow sections from different fabrication routes involving welding or combinations of welding and press-braking. Tensile coupon tests were conducted on the specimens extracted from different locations of the hollow sections with different fabrication routes and static mechanical properties and stress-strain relationship for the specimens were measured. The influence of welding on the material properties was found to be insignificant while strength enhancement was observed for the material at corners formed by press-braking. A stress-strain curve model was proposed for the material across octagonal high strength steel hollow sections. The magnitudes and distributions of longitudinal residual stresses of the octagonal high strength steel hollow sections with different fabrication routes were also measured using the sectioning method and were also found to be dependent on the fabrication route. Based on the measured residual stress results, residual stress models were developed for the hollow sections from different fabrication routes. The obtained variation of material properties and longitudinal residual stresses can be employed to accurately analyse the performance of octagonal high strength steel hollow section structural members for efficient structural designs.

Keywords

Octagonal hollow section; Material properties measurements; Residual stress; High strength steel; Fabrication route

1 Introduction

High strength steel (HSS) tubular members have been increasingly used in structural applications due to their combined advantages of strong buckling resistance, high strength-to-weight ratio, environmental efficiency, aesthetic appearance, and cost efficiency. Extensive experimental and numerical research studies focusing on HSS tubular structures with square, rectangular and circular sections have been conducted to determine the material properties and residual stresses of the hollow sections [1-6] and to investigate the cross-sectional and member behaviour under quasi-static compression, bending and combined loadings [1, 7-25]. In recent years, octagonal steel tubular members have also been used in civil structural applications such as transmission line structures, towers and lattice structures [26-28]. Octagonal hollow sections demonstrate stronger local buckling resistance than that of square and rectangular hollow sections and also provide the flat surfaces for the easier connection construction compared with circular hollow sections. Hence, HSS octagonal cross-section members have attracted the attention from researchers and structural manufacturers to apply the members in long-span truss structures [29-30]. In order to accurately predict the strength and behaviour of the HSS octagonal tubular members for efficient structural design, the variation of material properties and residual stresses in the HSS octagonal hollow sections which can influence the strength and buckling behaviour of the structures, need to be well understood.

The variation of properties and residual stresses existing in the members without being loaded are primarily induced by the structural fabrication processes [31-33]. Aoki et al. [34] investigated the compressive strength of octagonal steel tubular stub columns which were formed by welding eight steel plates, as depicted in Fig. 1(a). Godat et al. [26] used a different fabrication route by welding two half-sections to form octagonal tubular structures. In their study, each half-section had three cold-bended corners, as shown in Fig. 1(b). Mitiga et al. [35] and Migita and Fukumoto [36] also investigated the compressive strength of octagonal tubular structures produced using another fabrication route for which each half-section had four corners obtained by cold-bending, as shown in Fig. 1(c). In these fabrication routes, welding or combined welding and cold-bending processes were applied. Welding process induces heat-input to the materials around the welding seam and causes heat affected zone (HAZ) in which the material properties can be different from those of the materials outside HAZ [37]. Cold-bending process also affects the material properties due to strain hardening effect at the cold-bending region subject to large plastic deformations [32, 38-39]. Besides, the welding and cold-bending also lead to non-uniform thermal and plastic strains in the hollow section structural members and subsequently induce residual stresses. Since the buckling resistance and strength of the structures are dependent on the material properties and residual stresses, ignoring the variation of the properties and residual stresses in octagonal hollow sections can lead to inaccurate estimation of the structural performance. However, to date, no investigations have been performed to determine the variation of material properties and residual stresses in HSS octagonal hollow sections formed using the three different fabrication routes.

Therefore, in this study, the variation of material properties and residual stresses in HSS octagonal hollow sections formed using the aforementioned three fabrication routes are investigated experimentally. Tensile coupon tests were conducted on specimens extracted at different locations in the sections. The measured properties were compared in order to examine the effect of fabrication route on the variation of properties in the HSS octagonal hollow sections. Furthermore, residual stresses in the HSS octagonal hollow sections formed using the three fabrication routes were also measured and compared. The effect of fabrication route on the residual stress distribution in the sections is also discussed.

2 Octagonal hollow section specimens

HSS octagonal hollow section specimens were formed using the three fabrication routes introduced in Section 1. Specimens from the fabrication routes presented in Figs. 1(a)-(c) respectively are named W-Series, CF1-Series and CF2-Series. S690 steel plates with nominal yield strength of 690 N/mm^2 and with thicknesses of 6 and 10mm were used to form the specimens. The steel plates with each thickness were produced in the same batch, allowing the direct comparison of experimental investigations on the properties and residual stress of the specimens. For each specimen in W-Series, eight steel plates were welded together through gas metal arc welding (GMAW) and full penetration weld was used. The selected electrode wire was 1.2mm of the category ER110S-G according to the specification AWS A5.28 [40]. Preheating at about 150°C was applied prior to the start of each welding process. The applied shielding gas was Ar80%+$CO_2$20%. For the welding, the voltage was about 26-29V while the amperage was about 220-240A. While fabricating the specimens using the CF1 and CF2 routes, the steel plates were longitudinally folded at room temperature through press-braking to form the half octagonal sections. Two half octagonal sections were subsequently welded through GMAW to form each specimen in CF1 or CF2 series. Three cross-sectional dimensions were chosen for specimens with each fabrication route. The measured dimensions for the specimens with different plate thicknesses and plate width-to-thickness ratios between 6.7 and 23.7 are shown in Table 1 using the nomenclature defined in Fig. 1. The specimens are labelled based on the fabrication route and nominal dimensions. For example, the label "CF2-75×10" defines the specimen formed using fabrication route CF2 shown in Fig. 1(c) and with the nominal edge length (B) and thickness (t) of 75 and 10mm respectively.

3 Material properties investigations

3.1 Tensile coupon tests

Tensile coupon tests were conducted to measure the material properties of HSS octagonal hollow sections and to examine the heterogeneity in the material of the hollow sections due to fabrication processes. Longitudinal tensile coupons were taken from both flat and corner regions of the HSS octagonal hollow section specimens. During each tensile coupon test, the loading was paused near yield and ultimate strength for 90s to obtain the static loads [41]. Static stress-strain curves obtained from the tensile coupon tests were used to determine the static 0.2% proof stress ($\sigma_{0.2}$), static ultimate tensile strength (σ_u), modulus of elasticity (E), static ultimate tensile strain (ε_u) and elongation at fracture (ε_f) of the material.

3.1.1 Flat coupon tests

Flat tensile coupons were extracted from the centre of the faces of HSS octagonal hollow sections, as shown in Fig. 1. The dimensions of the flat coupons conformed to the EN10002-1 [42]. The coupons had 6 mm width along the gauge length. The test set-up of flat coupon is shown in Fig. 2(a). A calibrated mechanical extensometer was mounted onto each coupon specimen to measure the longitudinal strain during the test. Two linear strain gauges were also attached at the midpoint on each of the faces of any coupon specimen. The average strain measured by the two strain gauges was used to determine the modulus of elasticity for each coupon specimen. The strains and elongation at fracture (ε_f) measured using the extensometer enable the evaluation of material properties in general [1, 41]. By consistently applying this measurement methodology in tensile coupon tests, the variation of material properties in HSS octagonal hollow sections from different fabrication routes can be examined. The precise measurements of strain field at the necking region and fracture point appeared during a tensile coupon test requires the usage of special technique [43] such as digital image correlation (DIC). The strains and elongation of the coupon specimens were measured by strain gauges and extensometer, and DIC technique was not used in this research study. The static stress-strain curves for flat coupons obtained from different HSS octagonal hollow sections are presented in Fig. 3. The material properties determined from the static stress-strain curves in Fig. 3 are given in Table 2. The value of $\sigma_{0.2}$ for the coupon specimens ranges from 753 to 780 MPa while the σ_u varies from 795 to 821 MPa. For the HSS octagonal hollow sections with the same plate thickness, consistent stress-strain behaviour was obtained for the materials at the centre of the flat portions from these sections formed using different fabrication routes, as can be observed in Fig. 3. This observation indicates that the influence of welding and press-braking on materials at the centre of the flat faces was relatively insignificant due to the distances between the location of flat coupons and the welded or corner regions.

3.1.2 Corner coupon tests

Corner coupons were extracted from the corner regions of CF1 and CF2 series sections and the locations of the coupons in the sections are shown in Figs. 1(b) and (c). The width of the corner coupons is 4mm. For each corner coupon, two holes with the diameter of 8.5mm were drilled at a distance of 15mm from both ends of the coupon. The two holes were used for the installation of two specially fabricated pins for gripping the coupon specimen so that tensile loading can be applied to the corner coupon through its centroid [41], as shown in Fig. 2(b). The test procedures for the corner coupon tests are identical to those for the flat coupon tests. Static stress-strain curves were obtained, as presented in Fig. 4. The material properties determined based on these static stress-strain curves are summarised in Table 3. By comparing the stress-strain curves of corner coupons with those of flat coupons, the strength enhancement accompanied by the decrement of ductility can be clearly observed for the corner material due to the cold-working effect of the press-braking fabrication process. The $\sigma_{0.2}$ of each corner coupon was slightly larger than that of the flat coupon from the centreline of the face of the same HSS octagonal hollow section while the σ_u of the corner coupons was increased by 3 to 8% compared to that of the flat coupons. Contrary to the tensile strength enhancement, the ε_u of the corner coupons decreased significantly and was about 69 to 77% lower than that of the flat coupon from the same section. The ε_f for the corner coupons also decreased by 19 to 23%.

Both strength enhancement and reduction of ductility in corners with different ratios of inner corner radius over plate thickness (r_i/t) were also compared. For CF1-75×10 and CF2-75×10 sections with the r_i/t ratio of about 1.50, the static $\sigma_{0.2}$ and σ_u of the corner materials respectively increased by 2.7 and 7.6% on average compared with those of the material at the centre of the flat regions while the ε_u and ε_f decreased by 73.5% and 20.5% on average respectively. For CF1-75×6, CF1-160×6, CF2-75×6 and CF2-160×6 sections with r_i/t ratios ranging from 2.22 to 2.50, the static $\sigma_{0.2}$ and σ_u of the corner materials increased by 2.7 and 5.1% on average respectively while the ε_u and ε_f decreased by 73.2% and 20.5% on average respectively. Comparing the effect of press-braking fabrication on the material properties of corners with different r_i/t ratios, both the strength enhancement and reduction of ductility occurred at corners were insensitive to the r_i/t ratio. The minimal influence of r_i/t ratio was due to the relatively small differences between the r_i/t ratios of corners from different sections. Besides, the level of strain hardening for the high strength steel material is relatively low, as can be seen from the stress-strain curves in Fig. 3 for flat coupons. Thus, no obvious differences in both strength enhancements and reduction of ductility for the corner materials in different sections were obtained although the corners in CF1-75×10 and CF2-75×10 sections with lower r_i/t ratios may experience slightly larger plastic strains [44].

3.1.3 One-eighth and quarter section coupon tests

Differences between the mechanical properties of the material at the centre of the flat surface and those at the corners of CF1 and CF2 series HSS octagonal hollow sections were found, as presented in Sections 3.1.1 and 3.1.2. Thus, the material properties at different locations in the octagonal hollow sections are heterogeneous. As for the W series octagonal hollow sections, effect of welding on the material properties near the welding seam was also unknown. In order to examine the variation of material properties, especially the $\sigma_{0.2}$ and σ_u, around the HSS octagonal hollow sections, tensile coupons were taken for testing from different locations on one-eighth of W-75×6 section and on a quarter of CF1-75×6, CF2-75×6, CF2-75×10 and CF2-160×6 sections due to symmetrical geometry of the cross-sections. The location and labels of the tensile coupon specimens from these sections are presented in Figs. 5-9.

The measured static $\sigma_{0.2}$ and σ_u for the coupon specimens were plotted against the locations where the coupon specimens were extracted in each octagonal hollow section, as shown in Figs. 5-9. The tensile properties of the coupons from different HSS octagonal hollow sections are summarised in Table 4. As can be seen in the figures and Table 4, the tensile strength and ductility of the material at the weld are quite different from those of the material at the flat and corner regions of the hollow sections. The $\sigma_{0.2}$ is lower than that of the material at other different locations in HSS octagonal hollow sections while the elongation is much larger than that of the material at other locations in the hollow sections. This is because the width of the welding seam ranges from 8.5 to 11.3mm and is larger than the width of the middle part of each coupon specimen. Therefore, the part of each coupon under tensile loading during the tests was located well within the welding seam which had the infill of electrode material. Thus, the measured material properties at the weld depends on the properties of the electrode material and are different from the material properties of the steel plates at other locations in the hollow sections.

For the W-75×6 section, no obvious variation of material properties in the flat portions of the section was obtained, as shown in Fig. 5. The properties of the coupon specimens closest to the welding seams were compared with those of the coupon specimens at the centre of the flat faces for W-75×6 section as well as CF1 and CF2 series sections. As shown in Figs. 5-9 and Table 4, the influence of welding on the material properties near the welding seams is quite low. For the W-75×6, CF1-75×6 and CF2-75×6 sections, the static $\sigma_{0.2}$ and σ_u measured for the coupons near the welding seams respectively were found to be only 0.5-3% and 0.25-1.4% lower than those of the coupons at the centre of the flat faces in the sections. As for the CF2-75×10 and CF2-160×6 sections, no influence of welding on the $\sigma_{0.2}$ and σ_u of the material near the welding seam was observed. Since the differences between the properties of materials near the welding seams and those of the materials at the centre of flat faces are minimal, no influence of cooling rate after welding on the material properties of specimens closest to the welding seams is observed [45-46]. The influence of press-braking fabrication on the material properties in the CF1-75×6, CF2-75×6, CF2-75×10 and CF2-160×6 sections can also be revealed in Figs. 6-9 and Table 4. Highest strength enhancements occurred at the corners for these sections because the stresses and plastic deformations induced by press-braking process concentrated at the corner regions [38]. For CF1-75×6, CF2-75×6, CF2-75×10 and CF2-160×6 section respectively, the static $\sigma_{0.2}$ of corners increased by 2.3, 5.7, 1.9 and 2.8% on average compared with that of the material at the centre of the flat region while the static σ_u increased by 3.7, 4.9, 7.2 and 6.9% on average.

3.2 Proposed stress-strain curve model

The material stress-strain relationship is needed for the analysis and design of HSS octagonal hollow section structures. A stress-strain curve model is given in European standard [47] and describes the stress-strain relationship in the form of multi-linear curves. However, the variation of stress with increasing strain for the HSS material in the octagonal hollow sections, especially the material at the corners formed by press-braking, is non-linear when the stress is above the proportional limit and behaviour of the material becomes inelastic under loading, as shown in Figs. 3 and 4. Thus, using the stress-strain model in European standard can lead to inaccurate stress-strain relationship for structural design and analysis. In order to describe the non-linear stress-strain behaviour, Hill [48] proposed a stress-strain curve model based on the Ramberg and Osgood equation [49], as given as Eq. (1). The parameter n, as the strain hardening exponent is constant.

$$\varepsilon = \frac{\sigma}{E} + 0.002\left(\frac{\sigma}{\sigma_{0.2}}\right)^{n} \quad (1)$$

This model was found to provide suitable stress-strain curves up to $\sigma_{0.2}$ and overestimate the stress at the strains greater than 0.2% since the parameter n related to strain hardening may vary with increasing strains [2]. Therefore, a concept proposed by Mirambell and Real [50] of using two-stage Ramberg and Osgood equations to replicate the non-linear stress-strain behaviour was employed in this study. The two-stage Ramberg and Osgood material model [51] given as Eq. (2) was used to replicate the stress-strain relationship for the material at the flat and corner regions in HSS octagonal hollow sections.

$$\varepsilon = \begin{cases} \frac{\sigma}{E} + 0.002\left(\frac{\sigma}{\sigma_{0.2}}\right)^{n_1} & for\ \sigma \le \sigma_{0.2} \\ \frac{\sigma-\sigma_{0.2}}{E_{0.2}} + \left(\varepsilon_{tu} - \frac{\sigma_u-\sigma_{0.2}}{E_{0.2}} - \varepsilon_{t0.2}\right)\left(\frac{\sigma-\sigma_{0.2}}{\sigma_u-\sigma_{0.2}}\right)^{n_2} + \varepsilon_{t0.2} & for\ \sigma > \sigma_{0.2} \end{cases} \quad (2)$$

In the equation, $E_{0.2}$ is the stiffness at the $\sigma_{0.2}$, ε_{tu} is the strain at the ultimate strength, $\varepsilon_{t0.2}$ is the total strain at the $\sigma_{0.2}$, n_1 and n_2 are strain hardening exponents. Eqs. (3) and (4) are proposed for calculating the values of n_1 and n_2 respectively. In Eq. (3), $\sigma_{0.01}$ is the 0.01% proof stress. $E_{0.2}$ for estimating the stress-strain relationship can be calculated from Eq. (5).

$$n_1 = \begin{cases} \frac{\ln(^{0.2}/_{0.01})}{\ln(^{\sigma_{0.2}}/_{\sigma_{0.01}})} + \log_{\left(\frac{\sigma_u}{\sigma_{0.2}}\right)}\left(\frac{\varepsilon_{tu}}{0.002}\right) & for\ flat\ portion\ material \\ \frac{\ln(^{0.2}/_{0.01})}{\ln(^{\sigma_{0.2}}/_{\sigma_{0.01}})} & for\ corner\ material \end{cases} \quad (3)$$

$$n_2 = \frac{\ln(^{\varepsilon_{tu}}/_{\varepsilon_{t0.2}})}{\ln(^{\sigma_u}/_{\sigma_{0.2}})} \quad (4)$$

$$E_{0.2} = \frac{E}{1+\frac{0.002 n_1 E}{\sigma_{0.2}}} \quad (5)$$

The stress-strain curves for the material at flat and corner regions across octagonal hollow sections were estimated using the proposed model and compared with the curves from tensile coupon tests, as shown in Fig. 10. As can be seen in the figure, the estimated stress-strain curves compared well with the curves obtained from experiments. Therefore, the proposed stress-strain curve model can be applied to develop stress-strain curves for the design and analysis of the octagonal hollow section structural members formed using the fabrication routes in Fig. 1.

4 Residual stress investigations

Residual stresses existing in the HSS octagonal hollow sections in the unloaded state may cause premature yielding in part of the material around the hollow sections and subsequently influence the strength and stability of the HSS octagonal hollow section structures [2-3]. For the HSS octagonal hollow sections, the residual stresses can be caused by the fabrication processes including welding, press-braking and flame-cutting. Since the residual stresses in the longitudinal direction along the length of the structures have the most influence on the structural behaviour [2, 52], the magnitude and distribution of the longitudinal residual stresses were measured for the sections with different geometry properties and formed using the three fabrication routes shown in Fig. 1.

4.1 Residual stress measurement technique

Sectioning method was adopted in this investigation and applied to measure the residual stresses for W-75×6, CF1-75×6, CF2-75×6, CF2-75×10 and CF2-160×6 sections. The specimens prepared for measuring residual stresses are 300mm in length. During the preparation, one-eighth of W-75×6 and a quarter of CF1-75×6, CF2-75×6 and CF2-75×10 sections were marked into longitudinal strips of 10mm widths while a quarter of CF2-160×6 section was marked into longitudinal strips of 13mm widths. This arrangement was consistent with that for tensile coupon tests described in Section 3.1.3

because the distribution of residual stresses can be regarded to be symmetrical in the hollow sections with the symmetrical locations of corner regions and welding seams. The strain gauges of 3mm gauge length were then attached on both outer and inner surfaces of the longitudinal strips at the mid-length of each strip. Each strain gauge was also protected with the cover of water proof glue to avoid any contamination and damage in the strain gauge due to sectioning. Initial readings of strain gauges were recorded before the start of sectioning process. Subsequently, sectioning was performed using the wire cutting method and coolant was used to minimise the heat generation during sectioning, as presented in Fig. 11. After the completion of sectioning, the readings of strains were also taken for all longitudinal strips. The initial strain readings before the sectioning process and the final strain readings after sectioning were used to analyse the residual stresses in the HSS octagonal hollow sections, as explained in Section 4.2.

4.2 Measurement results and discussion

The residual strains on the outer and inner surfaces (ε_o and ε_i respectively) of each longitudinal strip were estimated as the differences between the measured strains before and after the sectioning process. For each strip, the ε_o was found to be different from ε_i, indicating that both membrane and bending residual stresses existed in the investigated HSS octagonal hollow sections. Therefore, these residual stresses were determined based on the ε_o and ε_i for W-75×6, CF1-75×6, CF2-75×6, CF2-75×10 and CF2-160×6 sections.

The residual stresses in the W-75×6 section were first calculated. The membrane residual stresses were calculated as the average of ε_o and ε_i multiplied by elastic modulus of the material. The bending residual stresses were calculated as the difference in ε_o and ε_i multiplied by elastic modulus since the bending residual stresses were suggested to vary linearly through the thickness [53] of welded sections. The magnitude and distribution of the calculated membrane residual stresses and bending residual stresses on the outer surfaces are presented in Fig. 12 in which the maximum residual stresses are marked. Positive and negative values indicate the tensile and compression residual stresses respectively. As can be seen in the figure, the membrane residual stresses are much larger than the bending residual stresses in the W-75×6 section. High tensile membrane residual stresses were obtained at the welding seam and its surrounding two strips while compressive membrane residual stresses were obtained at the other parts of the section. The compression bending residual stresses appeared along the outer surfaces of the one-eighth section. The membrane residual stresses ranged from 13 to 58 % of the $\sigma_{0.2}$. The maximum value of the tensile and compression membrane residual stress respectively were about 58 and 39% of the $\sigma_{0.2}$ of the material while the maximum bending residual stresses on the outer surface was about 7.5% of the $\sigma_{0.2}$.

The residual stresses in the CF1-75×6, CF2-75×6, CF2-75×10 and CF2-160×6 sections were also estimated. Different from the W-75×6 section, the variation of bending residual stresses through thickness for the sections formed using press-braking was found to be non-linear [52-55]. Rectangular stress block through thickness distribution was recommended [52-53] to be suitable for simulating the distribution of bending residual stresses through thickness for sections formed using press-braking and was adopted in this study for estimating the bending residual stresses for CF1-75×6, CF2-75×6, CF2-75×10 and CF2-160×6 sections based on the measured ε_o and ε_i. The obtained membrane residual stresses and bending residual stresses on the outer surface of the sections are presented in Figs. 13-16. For these sections made with folded plates using press-braking, large tensile bending residual stresses were obtained on the outer surface at the corners which experienced large plastic deformations during fabrication and their magnitudes were much larger than those of the bending residual stresses at the other locations of the outer surface. The maximum values of the tensile bending residual stresses in CF1-75×6, CF2-75×6, CF2-75×10 and CF2-160×6 sections respectively were 20, 20, 27 and 18% of the $\sigma_{0.2}$ of the material at corners. As for the membrane residual stresses, both tensile and compression stresses existed in the sections. The maximum magnitude of membrane residual stresses in CF1-75×6, CF2-75×6, CF2-75×10 and CF2-160×6 sections respectively were 20, 24, 26 and 45% of the $\sigma_{0.2}$ of the material at centre of flat proportions.

The magnitude and distribution of the membrane and bending residual stresses in the CF1-75×6 and CF2-75×6 sections are also compared with the residual stresses of W-75×6 section to reveal the influence of fabrication process on the residual stresses. The pattern of residual stresses shown in Fig. 12 for the W-75×6 section is quite different from that of the CF1-75×6 and CF2-75×6 sections shown in Figs. 13 and 14 respectively. In the CF1-75×6 and CF2-75×6 sections formed using press-braking, the maximum bending residual stresses were much larger than that of the W-75×6 section while the maximum membrane residual stresses were lower than that of the W-75×6 section. The different distributions and magnitudes of residual stresses in octagonal hollow sections formed using different fabrication routes indicate that the residual stresses measured for the hollow sections with the specific fabrication route should be used in the design and analysis of the structures.

4.3 Proposed residual stress models

The obtained residual stress measurement results were also used to develop membrane and bending residual stress models for HSS octagonal hollow sections. For the W-series section, the longitudinal membrane and bending residual stress distribution models were proposed, as presented in Fig. 17. The magnitudes of the residual stresses given in the models were obtained as the average membrane and bending residual stresses over different locations of the hollow section and given as the normalised values by the measured $\sigma_{0.2}$ of the material. The positive and negative signs in the figure represent tensile and compressive stresses. The bending residual stress for the outer surface of the hollow section is in compression, as shown in Fig. 17.

The distribution models for longitudinal membrane and bending residual stresses in CF1-series sections were also proposed based on the experimental results, as shown in Fig. 18. Multi-linear curves and constant values at corners were used to simulate the distribution pattern of membrane residual stresses in the CF1-series octagonal hollow sections. The magnitude of the membrane residual stress at any location in the model was given based on the measured stress value shown in Fig. 13. Constant tensile or compressive bending residual stresses on the outer surface of the flat and corner portions were provided since the variation of the bending residual stress magnitudes in the flat or corner regions was low, as shown in Fig. 13. For the CF2-series sections, the proposed longitudinal membrane and bending residual stress distribution models are presented in Fig. 19. Magnitudes of the membrane and bending residual stresses in the model were obtained as the average of the stresses measured at the specific location in the sections.

5 Conclusions

The material properties and residual stress distribution in HSS octagonal hollow section from three fabrication routes have been investigated experimentally. For each fabrication route involving welding or a combination of welding and press-braking processes, hollow sections with different dimensions and plate width-to-thickness ratios were used for the investigations. The effects of welding and press-braking on the material properties of the HSS octagonal hollow sections were investigated by conducting coupon tests on specimens extracted from different locations in the cross-sections. The mechanical properties of the materials in the hollow sections formed through welding eight steel plates were found to be insensitive to the welding process. The static $\sigma_{0.2}$ and σ_u measured for the coupons near the welding seams were less than 3% lower than the properties measured for the coupons at the centre of the flat faces in the sections. For the hollow sections formed using press-braking and welding, strength enhancements at the corners were observed. Comparing with the material properties measured for the flat coupons, the static 0.2% proof stress and ultimate tensile strength of the corner coupons increased up to 5.7 and 7.2% respectively, due to the cold-working of the press-braking process. A stress-strain curve model was developed and found to be capable of accurately estimating the material stress-strain relationship. The model can be used to obtain the stress-strain curves for structural design and analysis.

The distribution and magnitude of longitudinal residual stresses of HSS octagonal hollow sections from different fabrication routes were determined using the sectioning method. It was found that both membrane and bending residual stresses existed in the octagonal hollow sections and their magnitudes were determined and plotted. The results showed that the residual stress distribution and magnitudes of the section formed through welding are quite different from those of the sections formed using both press-braking and welding. For the section formed by welding eight steel plates, the membrane residual stresses ranged from 13% to 58% of the 0.2% proof stress of the material while the bending residual stresses were below 7.5% of the material 0.2% proof stress. As for the sections formed by combined press-braking and welding processes, the bending residual stresses in the flat regions were relatively low while the bending residual stresses at the corners which were subject to large plastic deformation during fabrication were quite large and found to be up to 27% of the 0.2% proof stress of the material at corners. The membrane residual stresses in these sections varied between 0.2 and 45% of the material 0.2% proof stress. Residual stress models for the HSS octagonal hollow sections formed using different fabrication routes were also proposed based on the experimental results.

Acknowledgements

The research work described in this paper was supported by a grant from the Research Grants Council of the Hong Kong Special Administrative Region, China (Project no. 15249216). The authors also appreciate the support from the Construction Industry Council and the Chinese National Engineering Research Centre for Steel Construction (Hong Kong Branch) at The Hong Kong Polytechnic University.

References

[1] Wang, J., Afshan, S., Schillo, N., Theofanous, M., Feldmann, M. and Gardner, L. 2017. Material properties and compressive local buckling response of high strength steel square and rectangular hollow sections. *Engineering Structures*, 130, 297-315.

[2] Ma, J.L., Chan, T.M. and Young, B. 2015. Material properties and residual stresses of cold-formed high strength steel hollow sections. *Journal of Constructional Steel Research*, 109, 152-165.

[3] Somodi, B. and Kövesdi, B. 2017. Residual stress measurements on cold-formed HSS hollow section columns. *Journal of Constructional Steel Research*, 128, 706-720.

[4] Yang, C., Yang, J.F., Su, M.Z. and Li, Y. 2017. Residual stresses in high-strength-steel welded circular tube. *Proceedings of the Institution of Civil Engineers*, 170, 631-640.

[5] Fatemeh, J., Heidarpour, A., Zhao, X.L., Hutchinson, C.R. and Minkkinen, J. 2016. Effect of weld on mechanical properties of high strength and ultra-high strength steel tubes in fabricated hybrid sections. *Engineering Structures*, 118, 16-27.

[6] Heidarpour, A., Tofts, N.S., Korayem, A.H., Zhao, X.L. and Hutchinson, C.R. 2014. Mechanical properties of very high strength steel at elevated temperatures. *Fire Safety Journal*, 64, 27-35.

[7] Shi, G., Zhou, W.J. and Lin, C.C. 2015. Experimental investigation on local buckling behaviour of 960 MPa high strength steel welded section stub columns. *Advances in Structural Engineering*, 18, 423-437.

[8] Ma, J.L., Chan, T.M. and Young, B. 2016. Experimental investigation on stub-column behaviour of cold-formed high strength steel tubular sections. *Journal of Structural Engineering*, 142(5), 04015174-1 to 04015174-11. ASCE.10.1061/(ASCE)ST.1943-541X.0001456.

[9] Yang, D.M. and Hancock, G.J. 2006. Numerical simulation of high-strength steel box-shaped columns failing in local and overall buckling modes. *Engineering Structures*, 132, 541-549.

[10] Rasmussen, K.J.R. and Hancock, G.J. 1995. Test of high strength steel columns. *Journal of Constructional Steel Research*, 34, 27-52.

[11] Wang, Y.B., Li, G.Q., Chen, S.W. and Sun, F.F. 2014. Experimental and numerical study on the behavior of axially compressed high strength steel box-columns. *Engineering Structures*, 58, 79-91.

[12] Ban, H.Y., Shi, G., Shi, Y.J. and Bradford, M.A. 2013. Experimental investigation of the overall buckling behaviour of 960 MPa high strength steel columns. *Journal of Constructional Steel Research*, 88, 256-266.

[13] Li, T.J., Li, G.Q., Chan, S.L. and Wang, Y.B. 2016. Behavior of Q690 high-strength steel columns: Part1: Experimental investigation. *Journal of Constructional Steel Research*, 123, 18-30.

[14] Li, T.J., Liu, S.W., Li, G.Q., Chan, S.L. and Wang, Y.B. 2016. Behavior of Q690 high-strength steel columns: Part2: Parametric study and design recommendation. *Journal of Constructional Steel Research*, 122, 379-394.

[15] Somodi, B. and Kövesdi, B. 2017. Flexural buckling resistance of cold-formed HSS hollow section members. *Journal of Constructional Steel Research*, 128, 179-192.

[16] Ma, J.L., Chan, T.M. and Young, B. 2016. Experimental investigation of cold-formed high strength steel tubular beams. *Engineering Structures*, 126, 200-209.

[17] Tran, A.T. 2016. Lateral-torsional buckling resistance of cold-formed high strength steel rectangular hollow beams. *In Proceedings of Sixth International Conference on Structural Engineering, Mechanics and Computation*, Cape Town, South Africa.

[18] Wang, J., Afshan, S., Gkantou, M., Theofanous, M., Baniotopoulos, C. and Gardner, L. 2016. Flexural behaviour of hot-finished high strength steel square and rectangular hollow sections. *Journal of Constructional Steel Research*, 121, 97-109.

[19] Pournara, A.E., Karamanos, S.A., Mecozzi, E. and Lucci, Antonio. 2017. Structural resistance of high-strength steel CHS members. *Journal of Constructional Steel Research*, 128, 152-165.

[20] Gkantou, M., Theofanous, M. and Baniotopoulos, C. 2017. Structural response of high strength steel hollow sections under combined biaxial bending and compression. In proceedings of *8th European Conference on Steel and Composite Structures*, Copenhagen, Denmark. p.3547-3556.

[21] Ma, J.L., Chan, T.M. and Young, B. 2017. Experimental investigation on cold-formed high strength steel circular hollow sections under combined compression and bending. In proceedings of *8th European Conference on Steel and Composite Structures*, Copenhagen, Denmark. p.3622-3630.

[22] Ma, J.L., Chan, T.M. and Young, B. 2017. Tests on high-strength steel hollow sections: a review. *Proceedings of the Institution of Civil Engineers – Structures and Buildings*, 170 (SB9), 621-630.

[23] Ma, J.L., Chan, T.M. and Young, B. 2018. Design of cold-formed high strength steel tubular stub columns. *Journal of Structural Engineering*, 144(6), 04018063.

[24] Fang, H. and Chan, T.M. 2018. Axial compressive strength of welded S460 steel columns at elevated temperatures. *Thin-walled Structures*, 129, 213-224.

[25] Nassirnia, M., Heidarpour, A., Zhao, X.L. and Minkkinen, J. 2015. A benchmark analytical approach for evaluating ultimate compressive strength of hollow corrugated stub columns. *Thin-walled Structures*, 117, 127-139.

[26] Godat, A., Legeron, F. and Bazonga, D. 2012. Stability investigation of local buckling behaviour of tubular polygon columns under concentric compression. *Thin-walled Structures*, 53, 131-140.

[27] Gonçalves, R. and Camotim, D. 2013. Elastic buckling of uniformly compressed thin-walled regular polygonal tubes. *Thin-walled Structures*, 71, 35-45.

[28] Zhu, J.Y. and Chan, T.M. 2018. Experimental investigation on octagonal concrete filled steel stub columns under uniaxial compression. *Journal of Constructional Steel Research*, 147, 457-467.

[29] Alechnavičius, V. and Bálint, J. 2014. Long span high strength steel trusses. Master thesis. Department of Civil, Environmental and Natural Resources Engineering, Luleå University of Technology.

[30] Manoleas, P., Koltsakis, E. and Veljkovic, M. 2017. Multiplanar K-joints on cold-formed open sections. In proceedings of *8th European Conference on Steel and Composite Structures*, Copenhagen, Denmark. p.629-638.

[31] Yu, W.W. and LaBoube, R.A. 2010. *Cold-formed steel design*. 4th Edition, Hoboken, USA: John Wiley & Sons, Inc.

[32] Sun, M. and Packer, J.A. 2014. Direct-formed and continuous-formed rectangular hollow sections - Comparison of static properties. *Journal of Constructional Steel Research*, 92, 67-78.

[33] Li, T.J., Li, G.Q. and Wang, Y.B. 2015. Residual stress tests of welded Q690 high-strength steel box- and H-sections. *Journal of Constructional Steel Research*, 20, 283-289.

[34] Aoki, T., Migita, Y. and Fukumoto, Y. 1991. Local buckling strength of closed polygon folded section columns. *Journal of Constructional Steel Research*, 20, 259-270.

[35] Migita, Y., Aoki, T., and Fukumoto, Y. 1992. Local and interaction buckling of polygonal section steel columns. *Journal of Structural Engineering*, 118, 2659-2676.

[36] Migita, Y. and Fukumoto, Y. 1997. Local buckling behaviour of polygonal sections. *Journal of Constructional Steel Research*, 41, 221-233.

[37] Sefcikova, K., Brtnik, T., Dolejs, J., Keltamaki, K. and Topilla, R. 2015. Mechanical properties of heat affected zone of high strength steels. *Material Science and Engineering*, 96, 012053.

[38] Cruise, R.B. and Gardner, L. 2008. Strength enhancements induced during cold forming of stainless steel sections. *Journal of Constructional Steel Research*, 64, 1310-1316.

[39] Quach, W.M. and Young, B. 2015. Material properties of cold-formed and hot-finished elliptical hollow sections. *Advances in Structural Engineering*, 18, 1101-1114.

[40] AWS A5.28/A5.28 M, 2005. Specification for Low-Alloy Steel Electrodes and Rods for Gas Shielded Arc Welding.

[41] Huang, Y. and Young, B. 2014. The art of coupon tests. *Journal of Constructional Steel Research*, 96, 159-175.

[42] EN 10002-1, 2001. *Metallic materials-Tensile testing-Part 1: Method of test at ambient temperature*. Brussels: European Committee for Standardization.

[43] Golling, S., Östlund, R. and Oldenburg, M. 2016. Characterization of ductile fracture properties of quench-hardenable boron steel: Influence of microstructure and processing conditions. *Material Science and Technology: A*, 658, 472-483.

[44] Rossi, B., Afshan, S. and Gardner, L. 2013. Strength enhancements in cold-formed structural sections - Part II: Predictive models. *Journal of Constructional Steel Research*, 83, 189-196.

[45] Keehan, E., Zachrisson, J. and Karlsson, L. 2010. Influence of cooling rate on microstructure and properties of high strength steel weld metal. *Science and Technology of Welding and Joining*, 15, 233-238.

[46] Hu, J., Du, L.X. and Wang, J.J. 2012. Effect of cooling procedure on microstructures and mechanical properties of hot-rolled Nb-Ti bainitic high strength steel. *Material Science and Engineering A*, 554, 79-85.

[47] EN 1993-1-1, 2005. *Eurocode 3: Design of steel structures - Part 1-1: General rules and rules for buildings*. Brussels: European Committee for Standardization.

[48] Hill, H.N. 1944. Determination of stress-strain relations from the offset yield strength values. Technical note no. 927. National Advisory Committee for Aeronautics. Washington, DC.

[49] Ramberg, W. and Osgood, W.R. 1943. Description of stress-strain curves by three parameters. Technical note no. 902. National Advisory Committee for Aeronautics. Washington, DC.

[50] Mirambell, E. and Real, E. 2000. On the calculation of deflections in structural stainless steel beams: an experimental and numerical investigation. *Journal of Constructional Steel Research*, 54, 109-133.

[51] Gardner, L. and Nethercot, D.A. 2004. Experiments on stainless steel hollow sections - Part 1: Material and cross-sectional behaviour. *Journal of Constructional Steel Research*, 60, 1291-1318.

[52] Cruise, R.B. and Gardner, L. 2008. Residual stress analysis of structural stainless steel sections. *Journal of Constructional Steel Research*, 64, 352-366.

[53] Gardner, L. and Cruise, R.B. 2009. Modeling of residual stresses in structural stainless steel sections. *Journal of Structural Engineering*, 135, 42-53.

[54] Quach, W.M., Teng, J.G. and Chung, K.F. 2006. Finite element predictions of residual stresses in press-braked thin-walled steel sections. *Engineering Structures*, 28, 1609-1619.

[55] Amouzegar, H., Schafer, B.W. and Tootkaboni, M. 2016. An incremental numerical method for calculation of residual stresses and strains in cold-formed steel members. *Thin-walled Structures*, 106, 61-74.

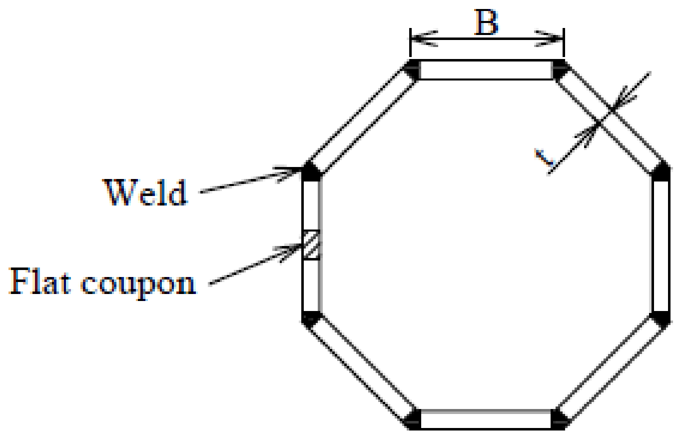

(a) W-series

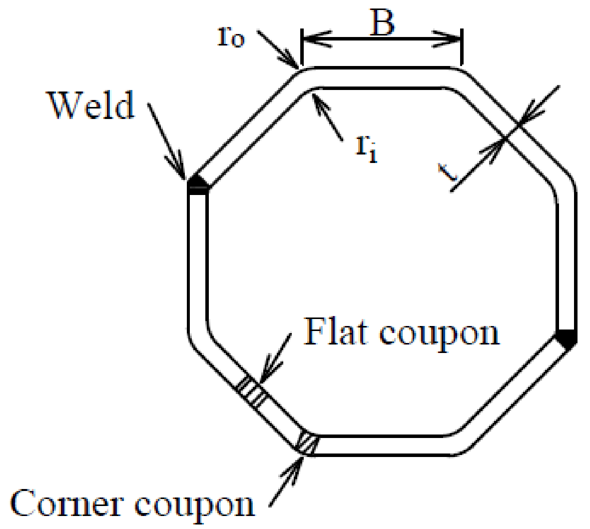

(b) CF1-series

Figure 1/19

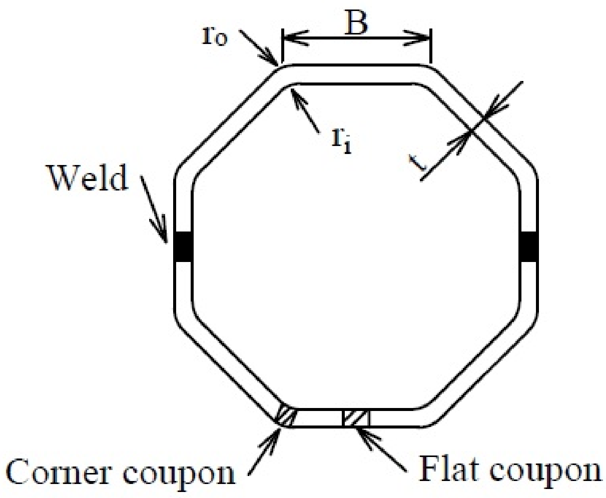

(c) CF2-series

Figure 1. Fabrication routes for octagonal steel hollow sections.

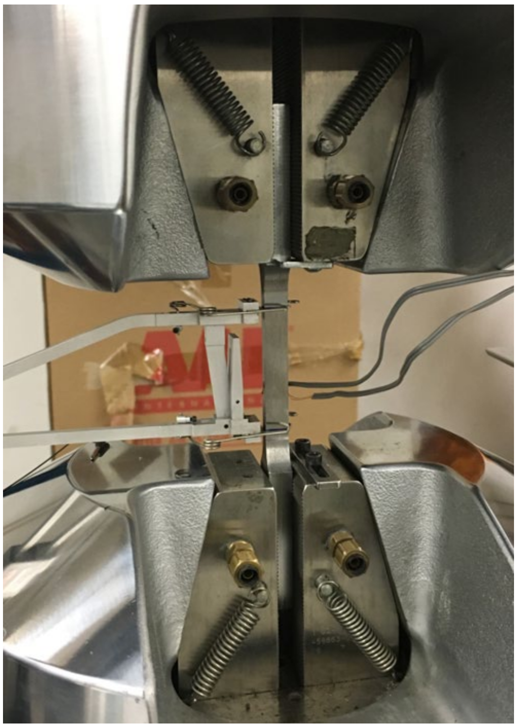

(a)

(b)

Figure 2. Set-up of tensile coupon test for (a) flat coupon and (b) corner coupon.

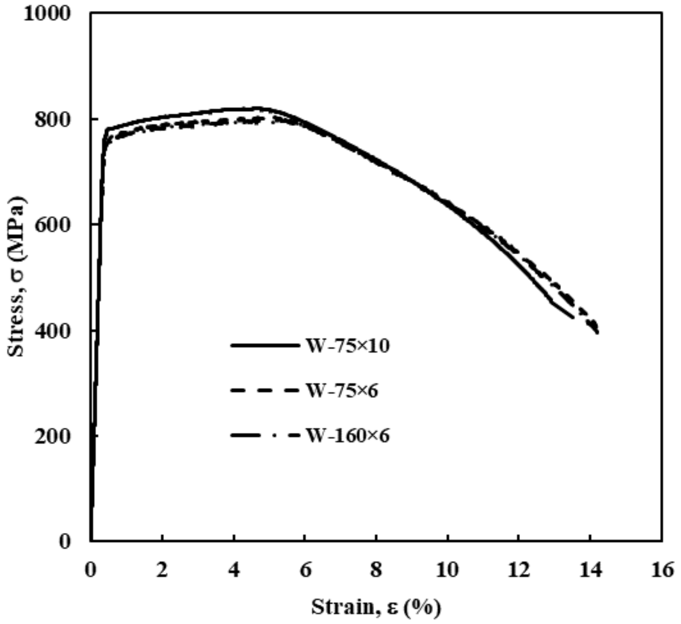

(a)

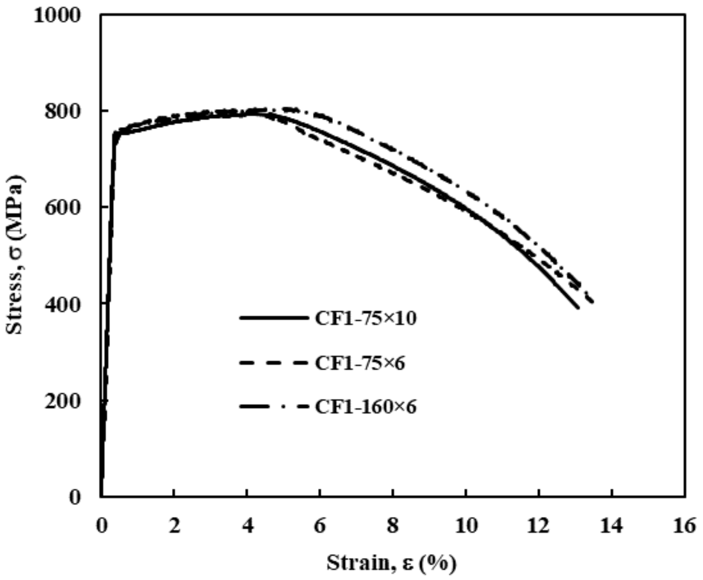

(b)

Figure 3/19

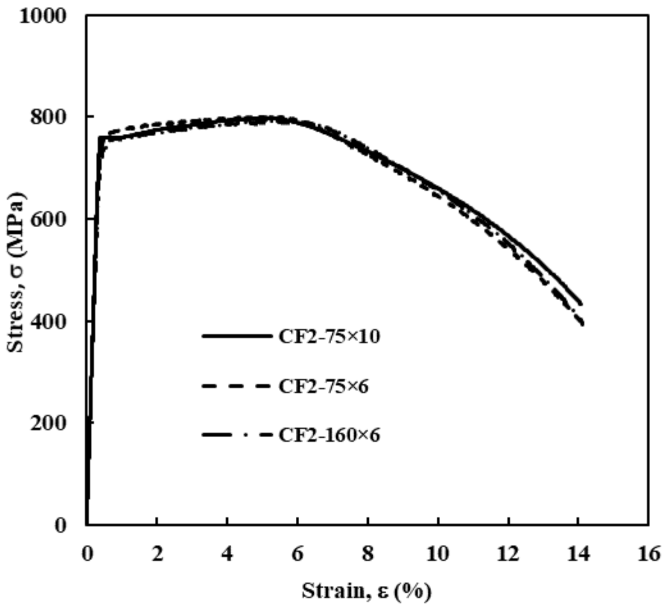

(c)

Figure 3. Measured static stress-strain curves for flat coupons obtained from (a) W series sections; (b) CF1 series sections and (c) CF2 series sections.

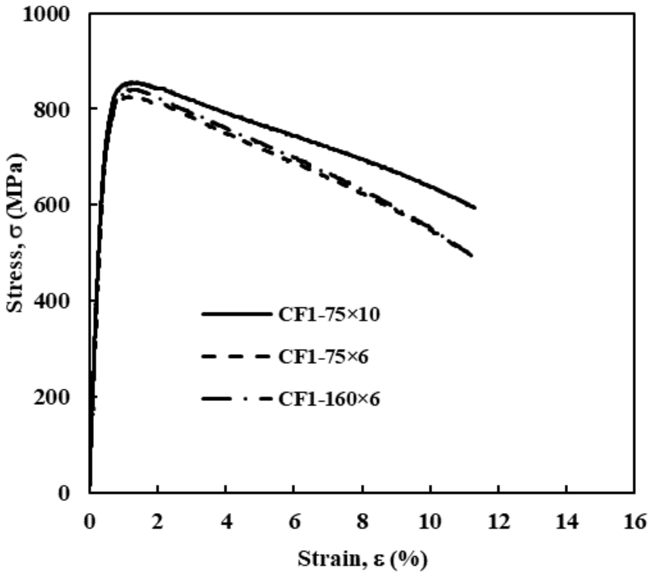

(a)

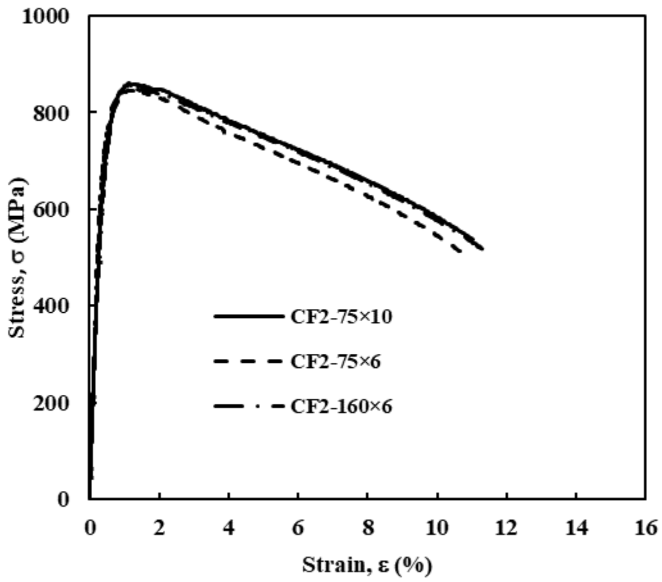

(b)

Figure 4. Measured static stress-strain curves for corner coupons obtained from (a) CF1 series sections and (b) CF2 series sections.

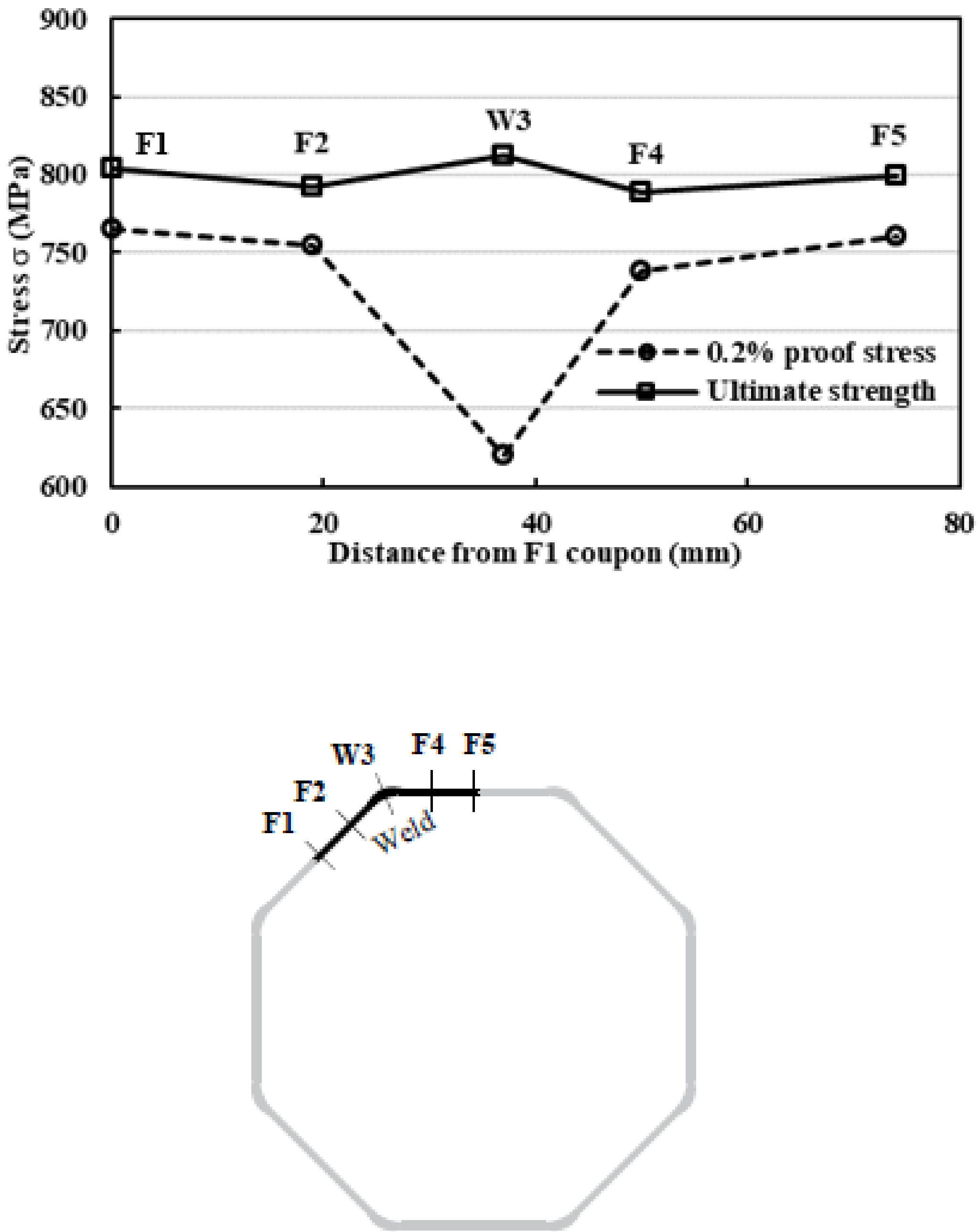

Figure 5. Variation of 0.2% proof stress ($\sigma_{0.2}$) and ultimate strength (σ_u) in W-75×6 section.

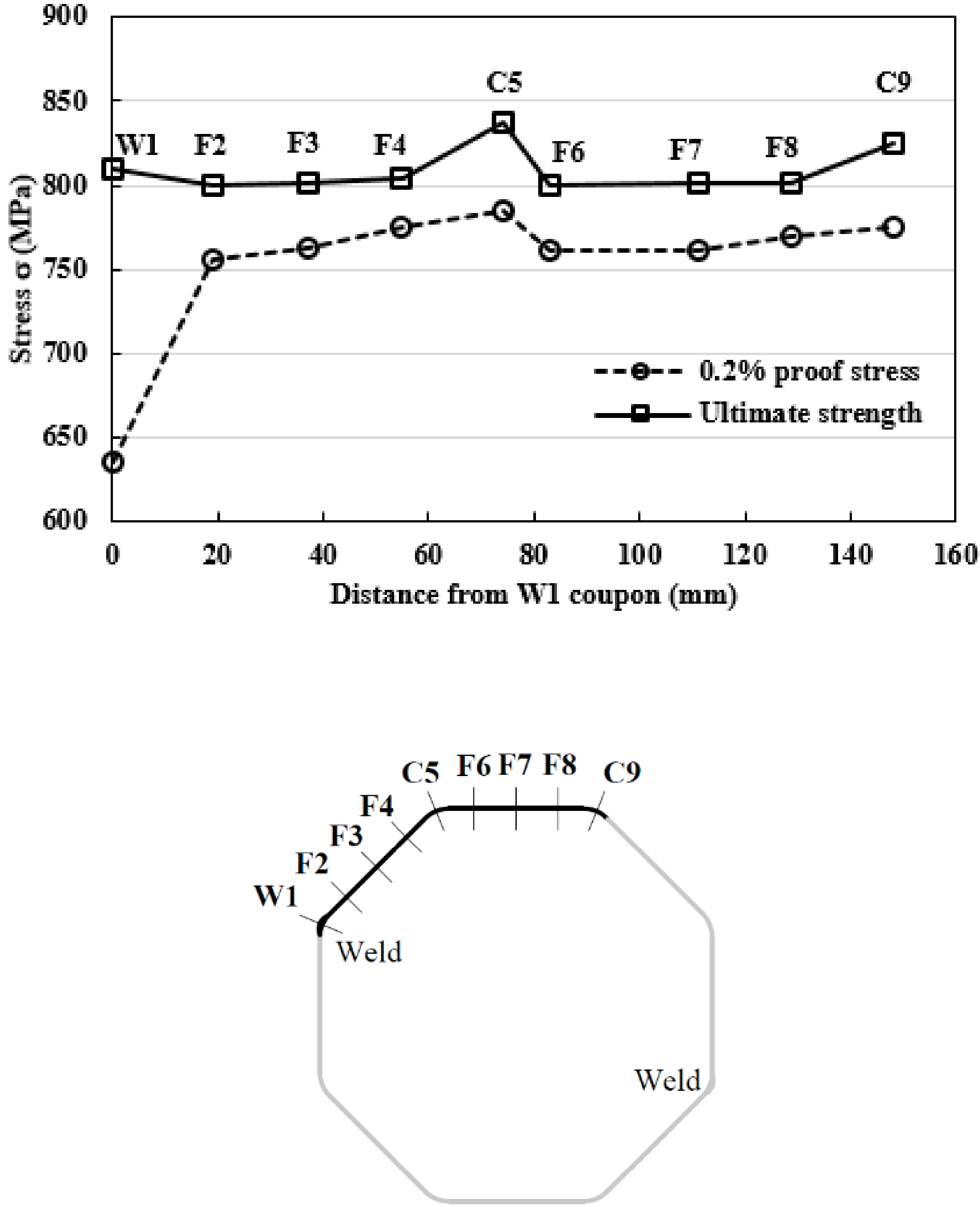

Figure 6. Variation of 0.2% proof stress ($\sigma_{0.2}$) and ultimate strength (σ_u) in CF1-75×6 section.

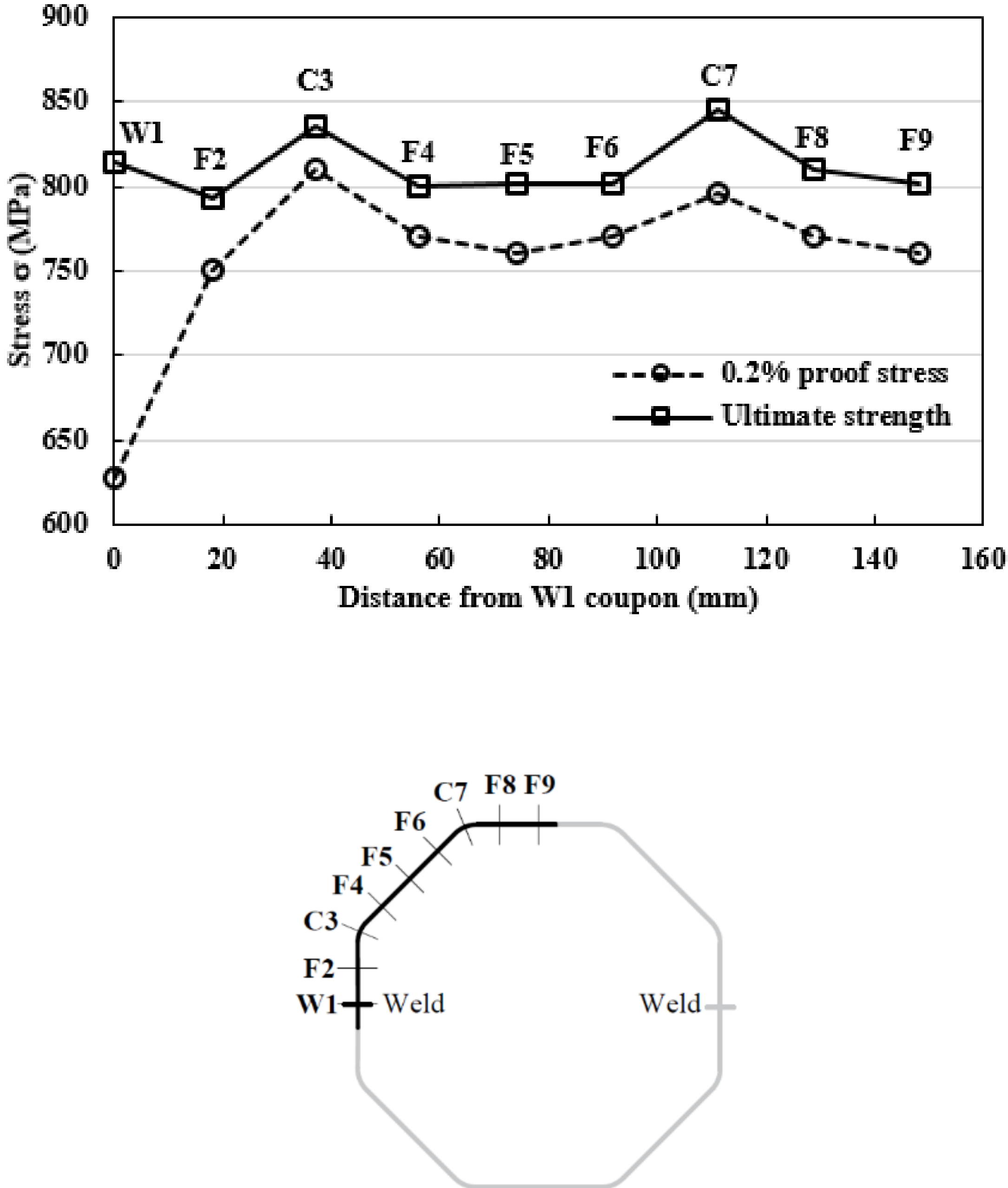

Figure 7. Variation of 0.2% proof stress ($\sigma_{0.2}$) and ultimate strength (σ_u) in CF2-75×6 section.

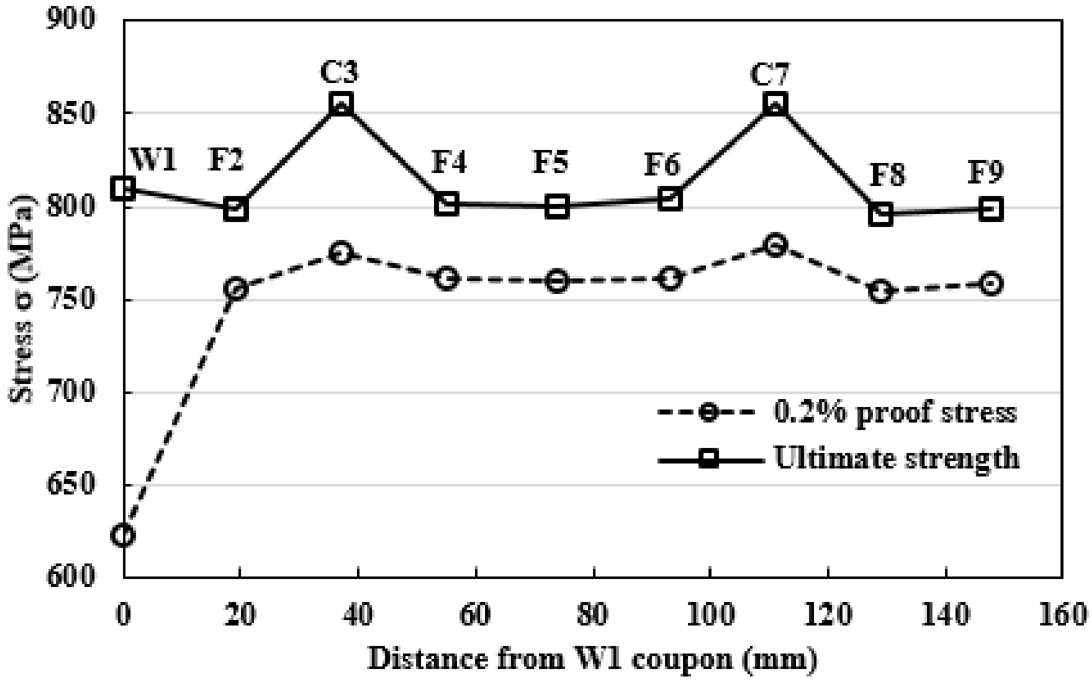

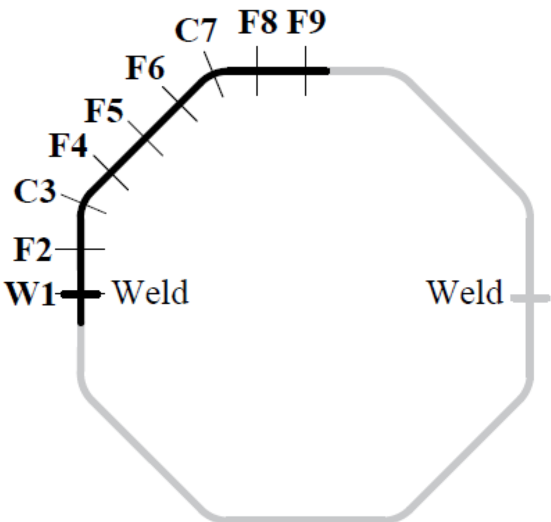

Figure 8. Variation of 0.2% proof stress ($\sigma_{0.2}$) and ultimate strength (σ_u) in CF2-75×10 section

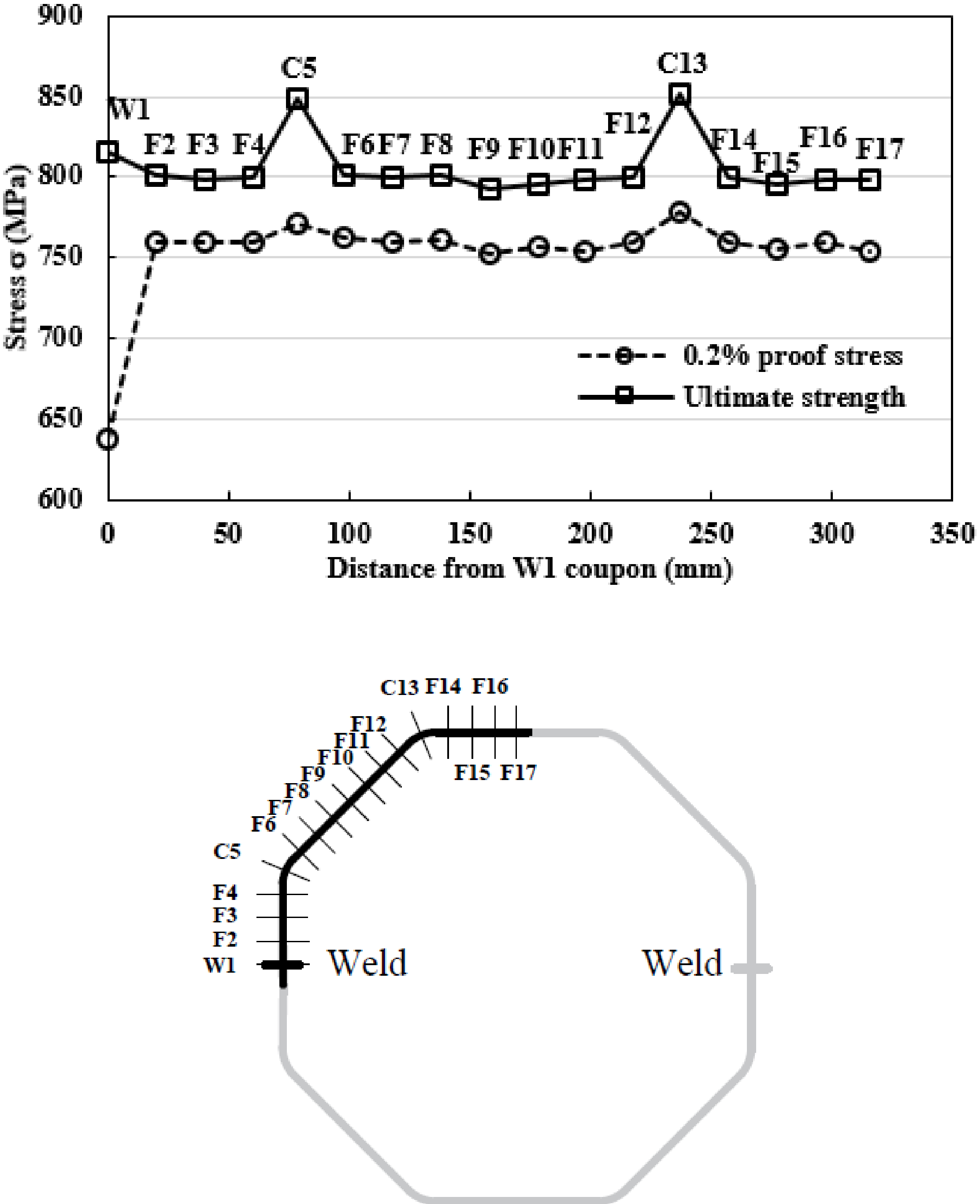

Figure 9. Variation of 0.2% proof stress ($\sigma_{0.2}$) and ultimate strength (σ_u) in CF2-160×6 section.

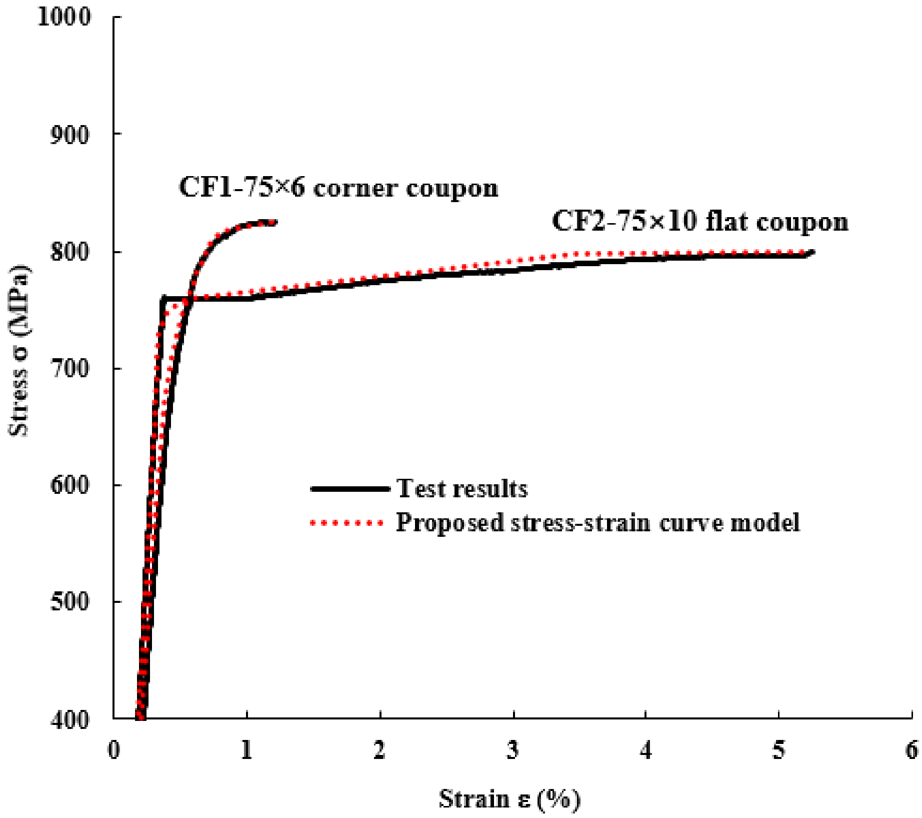

Figure 10. Comparison of stress–strain curves obtained from test results with the curves predicted using the proposed stress–strain curve model.

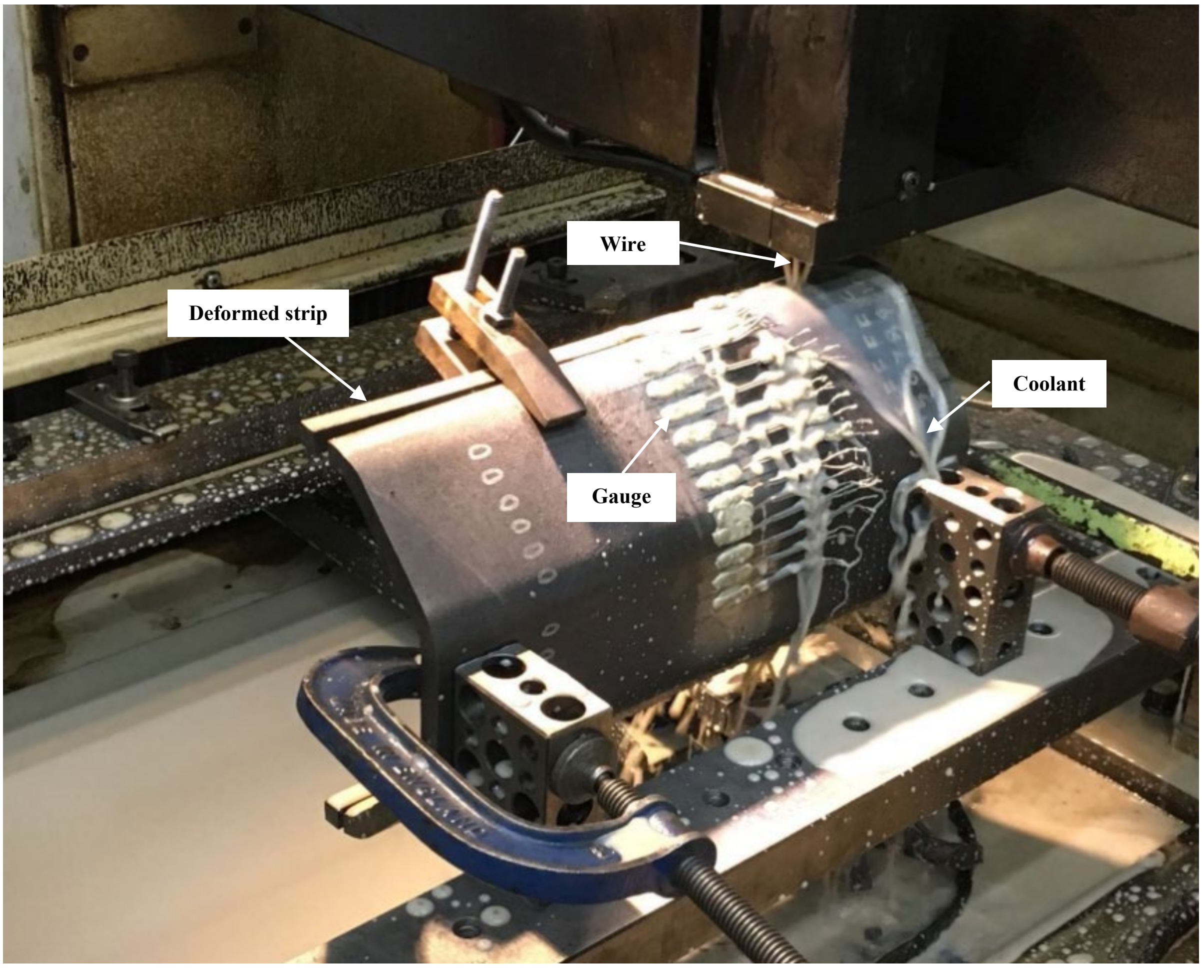

Figure 11. Sectioning process using wire-cutting with coolant.

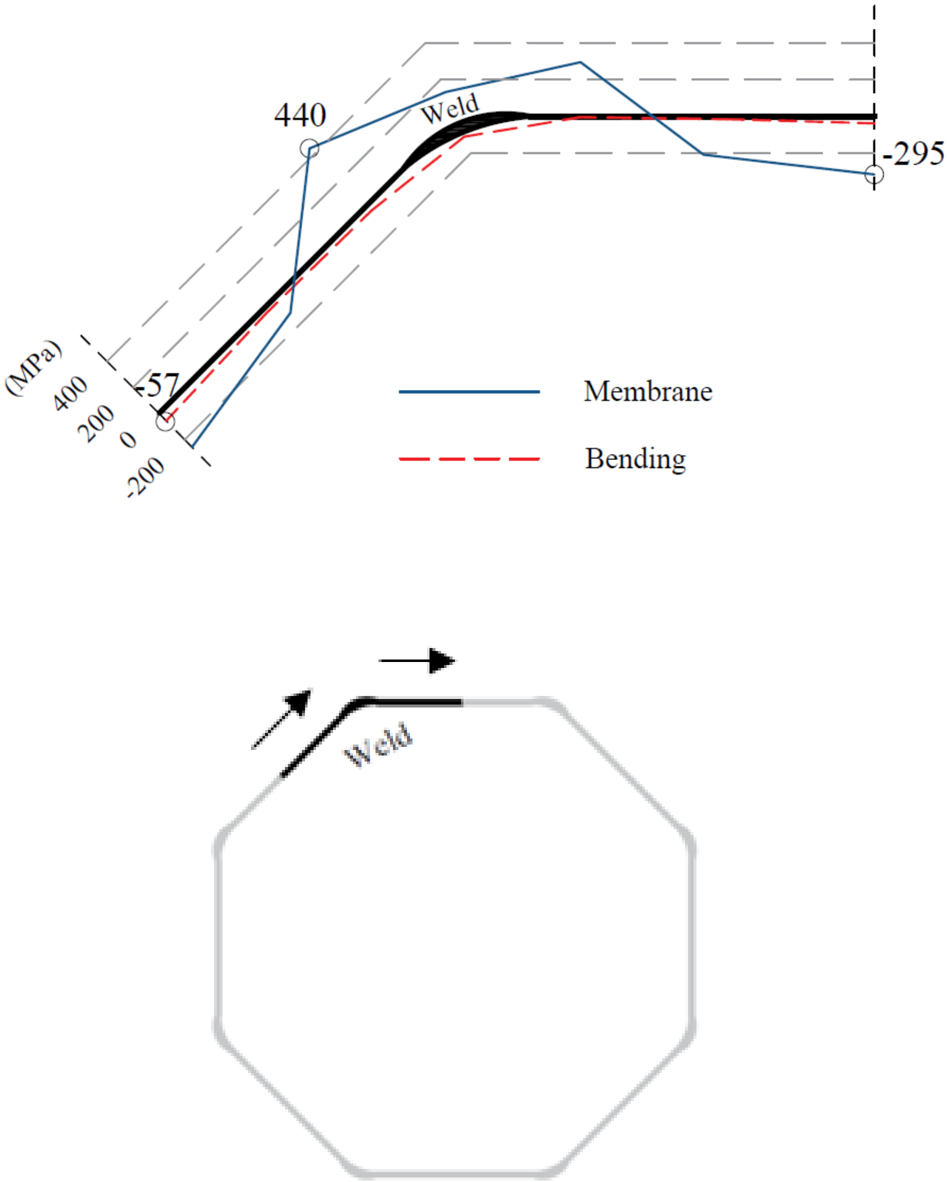

Figure 12. Membrane residual stresses and bending residual stresses on the outer surface along one-eighth of the W-75×6 section.

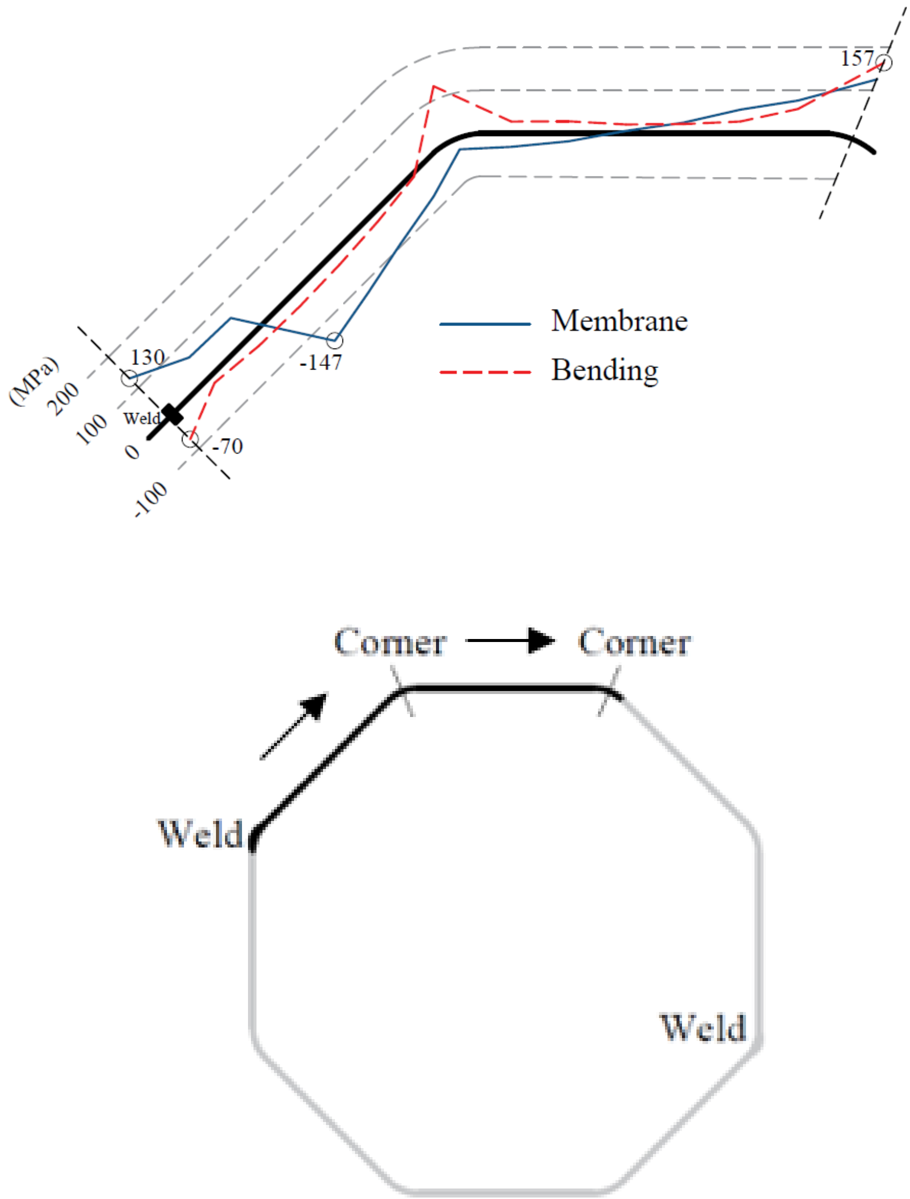

Figure 13. Membrane residual stresses and bending residual stresses on the outer surface along one-eighth of the CF1-75×6 section.

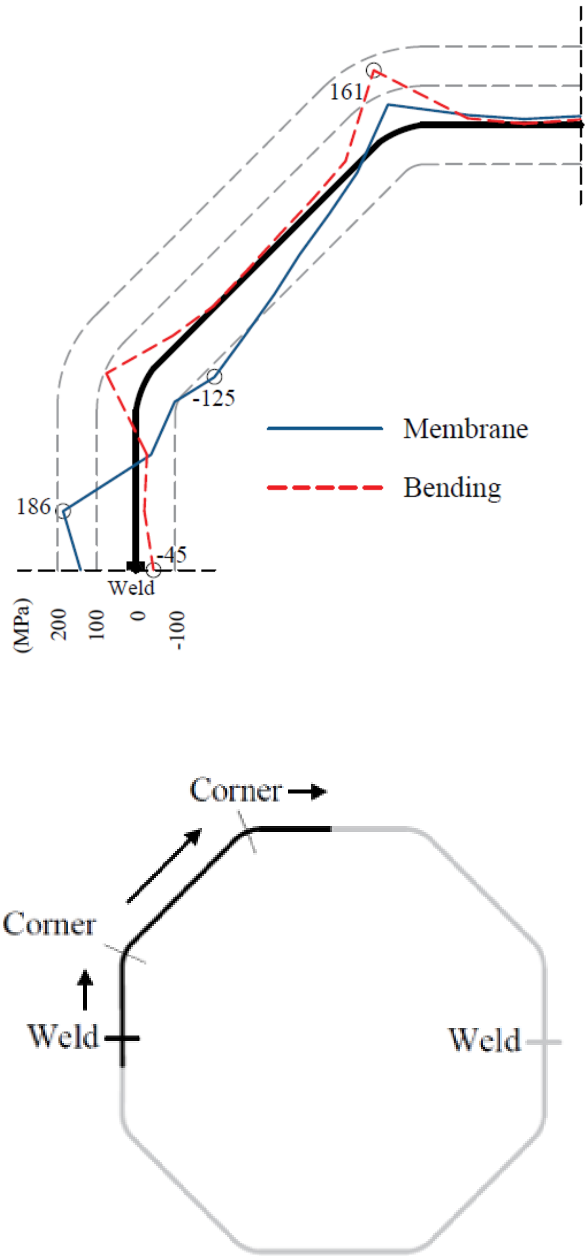

Figure 14. Membrane residual stresses and bending residual stresses on the outer surface along one-eighth of the CF2-75×6 section.

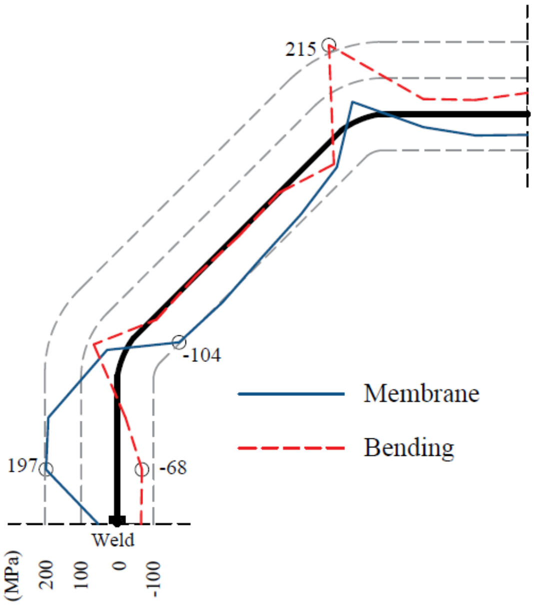

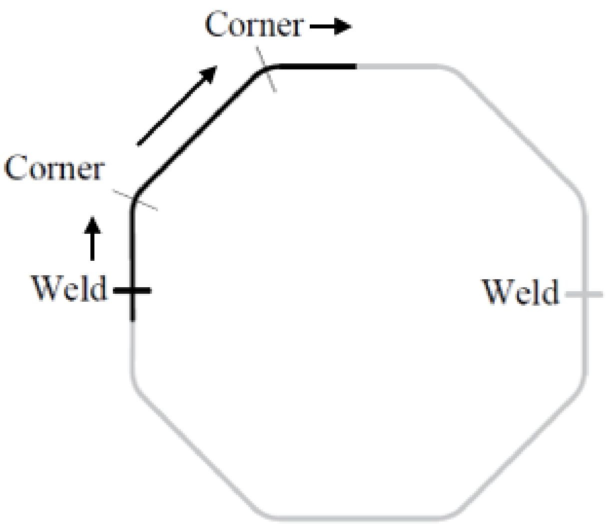

Figure 15. Membrane residual stresses and bending residual stresses on the outer surface along one-eighth of the CF2-75×10 section.

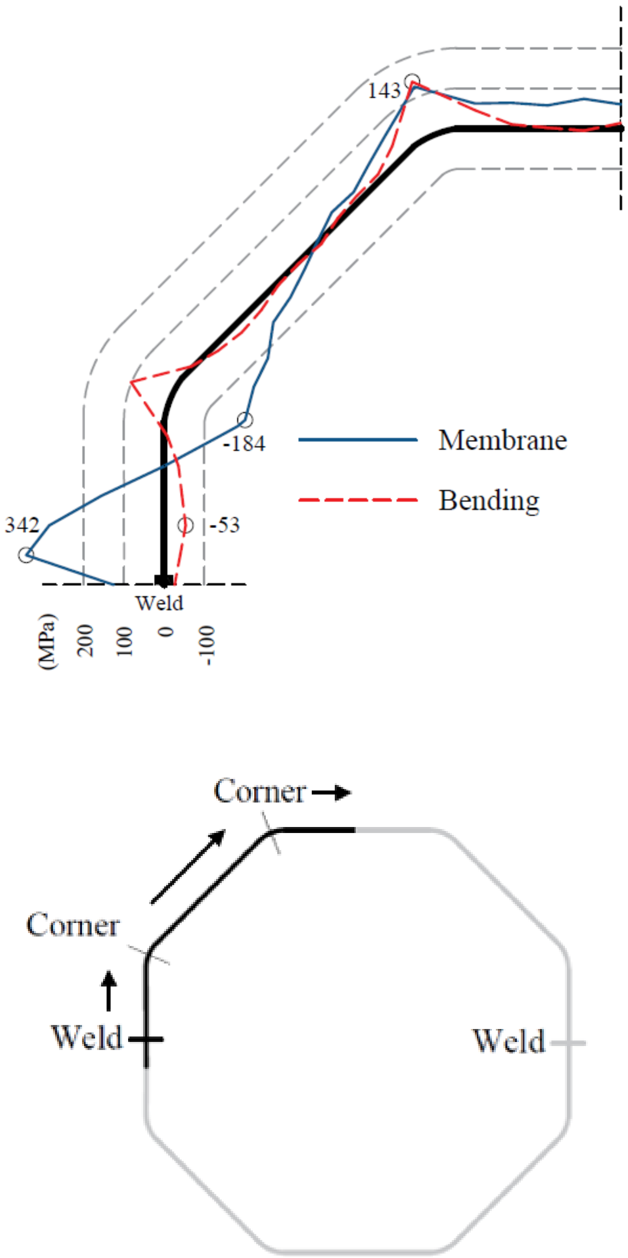

Figure 16. Membrane residual stresses and bending residual stresses on the outer surface along one-eighth of the CF2-160×6 section.

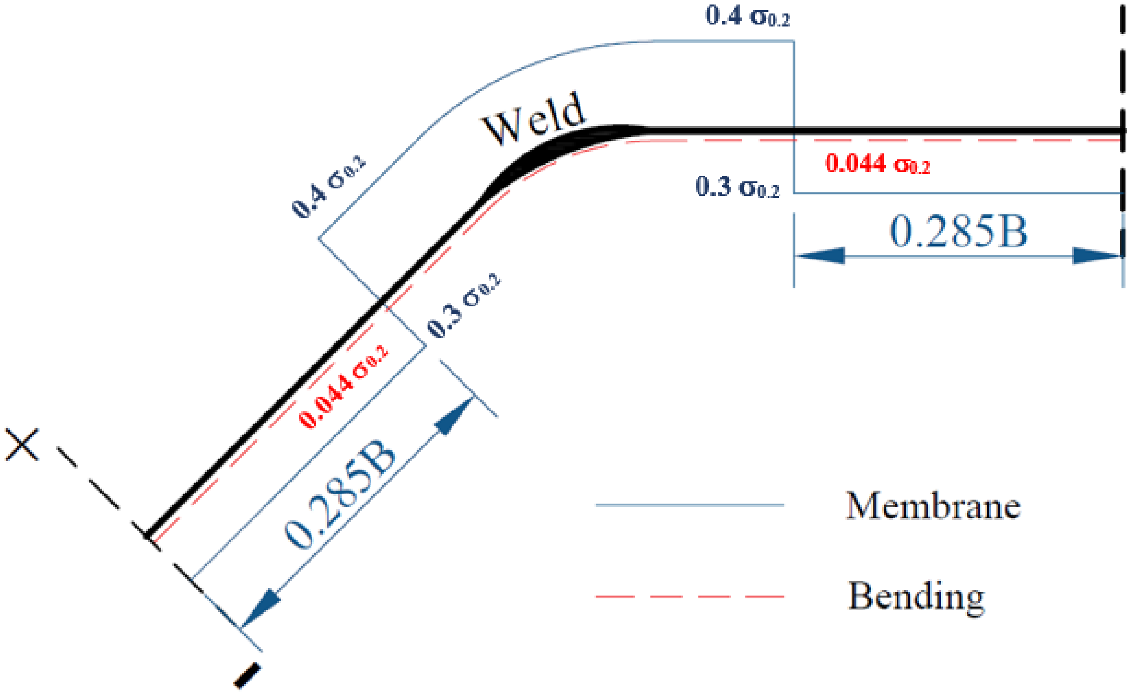

Figure 17. Residual stress distribution model for W-series sections.

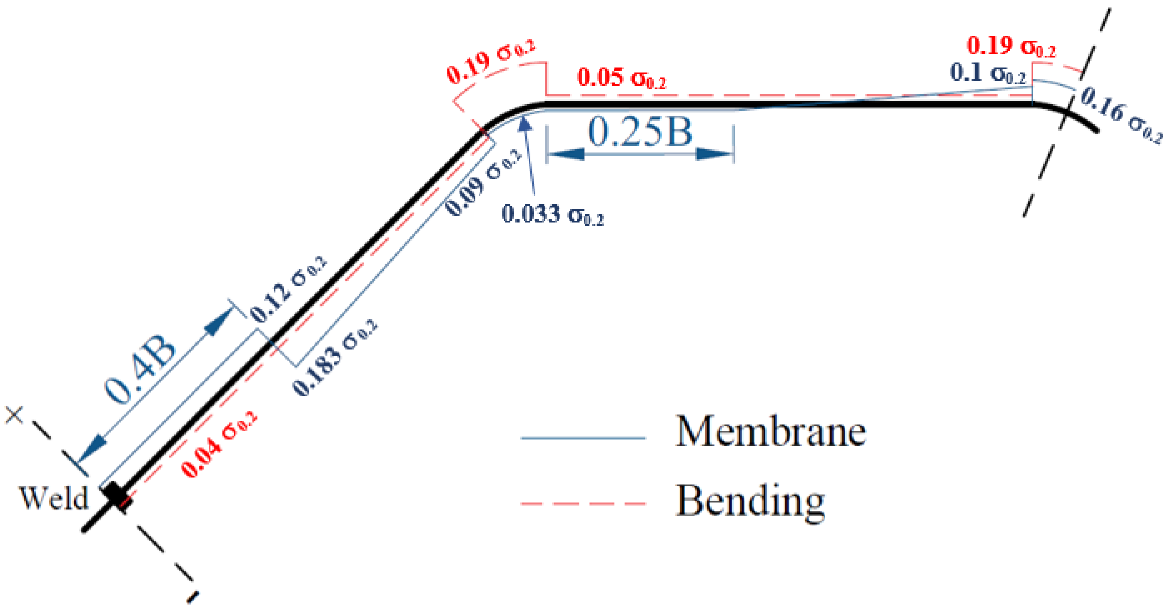

Figure 18. Residual stress distribution model for CF1-series sections.

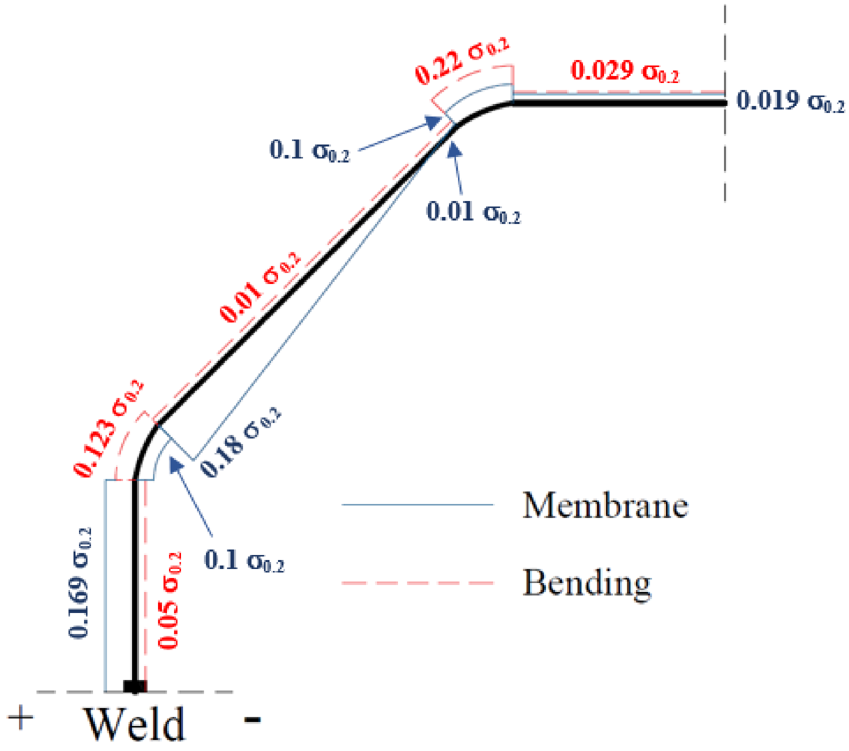

Figure 19. Residual stress distribution model for CF2-series sections.

Table 1. Dimensions of octagonal hollow sections.

Section	Edge length B (mm)	Thickness t (mm)	Outer corner radius r_o (mm)	Inner corner radius r_i (mm)
W-75×10	74.8	9.86	-	-
W-75×6	73.9	6.00	-	-
W-160×6	159.6	5.98	-	-
CF1-75×10	74.2	9.92	25.0	15.3
CF1-75×6	74.1	6.08	19.4	13.5
CF1-160×6	157.9	6.01	21.0	15.0
CF2-75×10	74.1	9.97	25.0	15.0
CF2-75×6	74.5	6.10	20.2	14.0
CF2-160×6	159.7	6.02	20.3	14.3

Table 2. Flat tensile coupon test results.

Section	**E (GPa)**	**$\sigma_{0.2}$ (MPa)**	**σ_u (MPa)**	**ε_u (%)**	**ε_f (%)**
W-75×10	215	780	821	4.6	13.5
W-75×6	214	764	804	4.5	14.2
W-160×6	213	764	808	4.7	14.2
CF1-75×10	215	753	795	4.6	14.0
CF1-75×6	210	762	802	4.1	13.7
CF1-160×6	215	766	805	5.1	13.5
CF2-75×10	216	759	799	5.3	14.1
CF2-75×6	215	760	801	4.5	14.1
CF2-160×6	215	754	798	5.0	14.1

Table 3. Corner tensile coupon test results.

Section	E (GPa)	$\sigma_{0.2}$ (MPa)	σ_u (MPa)	ε_u (%)	ε_f (%)
CF1-75×10	202	780	856	1.4	11.3
CF1-75×6	191	775	825	1.2	10.9
CF1-160×6	192	775	841	1.3	11.4
CF2-75×10	201	773	859	1.2	11.0
CF2-75×6	200	796	845	1.1	10.9
CF2-160×6	192	778	852	1.4	11.2

Table 4. Static mechanical properties measured for coupons taken from different locations of one-eighth of W-75×6 section and of a quarter of CF1-75×6, CF2-75×6, CF2-75×10 and CF2-160×6 sections.

Section	Coupon	E (GPa)	$\sigma_{0.2}$ (MPa)	σ_u (MPa)	ε_u (%)	ε_f (%)
W-75×6	F1	214	765	804	4.5	14.1
	F2	212	755	793	3.7	13.3
	W3	200	621	811	12.7	22.1
	F4	215	738	789	4.2	13.2
	F5	214	761	800	4.5	14.1
CF1-75×6	W1	202	635	810	12.5	22.2
	F2	214	756	800	3.7	12.0
	F3	210	763	802	3.8	13.6
	F4	214	775	804	4.0	12.6
	C5	190	785	838	1.4	11.0
	F6	213	762	800	4.0	12.5
	F7	212	762	802	4.1	13.8
	F8	210	770	802	3.7	12.5
	C9	191	775	825	1.2	10.9

CF2-75×6	W1	199	628	814	12.3	21.5
	F2	215	751	793	4.5	12.0
	C3	200	810	835	1.4	11.1
	F4	211	770	800	4.5	12.6
	F5	213	760	801	4.5	13.4
	F6	210	771	801	2.5	11.8
	C7	200	796	845	1.1	10.9
	F8	214	770	810	4.1	11.3
	F9	214	760	801	4.5	13.9
CF2-75×10	W1	195	623	810	11.9	21.3
	F2	214	756	799	4.7	13.8
	C3	202	775	855	1.3	11.1
	F4	215	762	801	4.9	13.4
	F5	215	760	800	4.3	13.0
	F6	216	761	804	5.1	13.5
	C7	201	773	859	1.2	11.0
	F8	215	754	796	4.6	13.5

Table 4/4

	F9	216	759	799	5.3	14.1
CF2-160×6	W1	198	638	815	13.0	22.6
	F2	213	760	801	3.9	12.5
	F3	214	760	799	4.0	13.4
	F4	211	759	800	3.8	12.9
	C5	195	771	848	1.2	10.9
	F6	214	762	801	3.7	12.7
	F7	211	760	800	4.0	13.2
	F8	210	761	801	4.4	13.6
	F9	211	753	793	4.2	13.0
	F10	212	757	795	4.3	13.2
	F11	209	754	799	3.6	12.6
	F12	210	760	800	4.2	12.8
	C13	192	778	852	1.4	11.2
	F14	210	760	800	4.9	14.0
	F15	208	756	795	4.5	13.7
	F16	209	760	798	4.3	13.8

Table 4/4

	F17	215	754	798	5.0	14.1

Table 4/4